

## Supporting Information

# An NIR fluorescent/photoacoustic dual-mode probe of NADPH for tumor imaging

Liandi Guan,<sup>a</sup> Wanting Hu,<sup>a</sup> Hongzhi Zuo,<sup>b</sup> Hua Sun,<sup>a</sup> Yongjian Ai,<sup>a</sup> Meng-qi He,<sup>a</sup> Cheng Ma,<sup>\*b</sup>

Mingyu Ding,<sup>\*a</sup> Qionglin Liang<sup>\*a</sup>

*a. MOE Key Laboratory of Bioorganic Phosphorus Chemistry & Chemical Biology, Department of Chemistry, Laboratory of Flexible Electronics Technology, Center for Synthetic and Systems Biology, Tsinghua University, Beijing 100084, P.R. China.*

*b. Department of Electronic Engineering, Tsinghua University, Beijing 100084, China.*

\*Corresponding author: Cheng Ma ([cheng\\_ma@tsinghua.edu.cn](mailto:cheng_ma@tsinghua.edu.cn)); Mingyu Ding ([dingmy@mail.tsinghua.edu.cn](mailto:dingmy@mail.tsinghua.edu.cn)); Qionglin Liang ([liangql@tsinghua.edu.cn](mailto:liangql@tsinghua.edu.cn))

<b>Experimental</b> .....	4
<b>Materials and Chemicals</b> .....	4
<b>Apparatus</b> .....	4
Synthesis of DD-QL .....	4
Synthesis of Rh-DD-Q .....	5
Synthesis of Rh-DD-QL .....	5
<i>In Vitro</i> Detection of NAD(P)H .....	6
Measurement of quantum yield .....	6
Cell Culture and Cytotoxicity Test .....	7
Fluorescence Imaging in living cells .....	7
Tumor Mouse Model .....	7
Fluorescence and Photoacoustic Imaging <i>in vivo</i> .....	8
Histology analysis .....	8
<b>Scheme S1.</b> Proposed mechanism of probe Rh-DD-QL response to NADPH .....	9
<b>Figure S1.</b> <sup>1</sup> H NMR spectra of compound DD-QL .....	10
<b>Figure S2.</b> <sup>13</sup> C NMR spectra of compound DD-QL .....	10
<b>Figure S3.</b> ESI-MS spectra of compound DD-QL .....	11
<b>Figure S4.</b> <sup>1</sup> H NMR spectra of compound Rh-DD-Q .....	11
<b>Figure S5.</b> <sup>13</sup> C NMR spectra of compound Rh-DD-Q .....	12
<b>Figure S6.</b> ESI-MS spectra of compound Rh-DD-Q .....	12
<b>Figure S7.</b> <sup>1</sup> H NMR spectra of compound Rh-DD-QL .....	13
<b>Figure S8.</b> <sup>13</sup> C NMR spectra of compound Rh-DD-QL .....	13
<b>Figure S9.</b> ESI-MS spectra of compound Rh-DD-QL .....	14
<b>Figure S10.</b> Line profile analysis for the time-dependent UV-vis absorption intensity changes of Rh-DD-QL .....	14
<b>Figure S11.</b> Dose-dependent UV-vis absorption spectrum changes of Rh-DD-QL .....	14
<b>Figure S12.</b> Fluorescence intensity changes of Rh-DD-QL with NAD(P)H .....	15
<b>Figure S13.</b> Fluorescence intensity changes of Rh-DD-QL with NAD(P)H at 825 nm .....	15
<b>Figure S14.</b> Relative absorption intensity of Rh-DD-QL at 790 nm in the presence of various analytes .....	15
<b>Figure S15.</b> UV-vis absorption spectrum of Rh-DD-QL with NADPH and other substances .....	16
<b>Figure S16.</b> Fluorescence-emission spectra of Rh-DD-QL with NADPH and other substances .....	16
<b>Figure S17.</b> Photoacoustic spectrum of Rh-DD-QL with NADPH and other substances .....	16
<b>Figure S18.</b> Fluorescence-emission spectra of Rh-DD-QL in the presence of various analytes with NADPH .....	17
<b>Figure S19.</b> Relative Fluorescence intensity of Rh-DD-QL in the presence of various analytes with NADPH .....	17
<b>Figure S20.</b> Photoacoustic spectra of Rh-DD-QL in the presence of various analytes with NADPH .....	17
<b>Figure S21.</b> Fluorescence-emission of Rh-DD-QL at different pH values in the presence of NADPH .....	18
<b>Figure S22.</b> HPLC-MS spectrogram of Rh-DD-QL before addition of NADPH .....	18

<b>Figure S23.</b> HPLC-MS spectrogram of Rh-DD-QL after addition of NADPH.....	18-19
<b>Figure S24.</b> Relative abundance of Rh-DD-QL and Rh-DD-QLR after incubation with 0, 1, 2, and 3 equivalents NADPH.....	19
<b>Figure S25.</b> Cytotoxicity Assays of probe Rh-DD-QL.....	19
<b>Figure S26.</b> The time-dependence of cellular fluorescence images and the fluorescence intensity of 4T1 cells.....	19-20
<b>Figure S27.</b> Fluorescence images and intensities of probe-stained 4T1 cells cultured at normal and hypoxia atmosphere.....	20
<b>Figure S28.</b> Relative fluorescence intensity of normal mice (H1, H2, H3) and tumor-bearing mice (C1, C2, C3) in Figure 4A.....	20
<b>Figure S29.</b> Time-dependent photoacoustic intensity variation trend in Figure 4C.....	20
<b>Figure S30.</b> Time-dependent fluorescence intensity variation trend of tumor locations in Group C2 and Group C4 in Figure 4B.....	21
<b>Figure S31.</b> H&E-stained histological analysis of the mice.....	21

## Experimental

### Materials and Chemicals

All the reagents and chemicals in the analytical grade were purchased from commercial suppliers and used without further purification. Beta-NAD(P)H, Beta-NAD(P)<sup>+</sup>, ATP, and ADP were purchased from Bide Pharmatech Ltd. (Shanghai, China). 4-diethylaminoketonic acid, cyclohexanone, 3-aldehyde quinoline, and methyl iodide (CH<sub>3</sub>I) were obtained from Energy Chemical. Epigallocatechin gallate, (1,3-Dioxolan-2-ylmethyl)triphenylphosphonium bromide, and 2-(2-Methoxyethoxy)-N,N-bis[2-(2-methoxyethoxy)ethyl]ethanamine was purchased from MERYER Co.,Ltd. (Shanghai, China). Cell culture media DMEM was obtained from Thermo Fisher Technology Co., Ltd (Shanghai, China). Mito-Tracker Green FM (50 μL) was purchased from Shanghai Yuanye Bio-Technology Co., Ltd (Shanghai, China). Reagents used for HPLC-MS detection were HPLC-MS grade. The cell culture dishes were purchased from NEST Biotechnology (Wuxi, China). All chemicals were used as received without further purification.

### Apparatus

<sup>1</sup>H NMR spectra were collected on a JNM-ECA400 NMR system or JNM-ECS600 NMR system (JEOL, Japan), and tetramethyl silane (TMS) was used as the internal standard. Mass spectral data were recorded on Q Exactive Orbitrap Mass Spectrometers (Thermo Fisher, USA). UV-vis absorption spectra were recorded on a UV-6100 ultraviolet spectrophotometer (Shanghai Meiputa instrument Co., Ltd) and an EnVision Multilabel Reader (PerkinElmer, USA), and fluorescence spectra were performed on a FluoroMax fluorescence spectrometer (HORIBA Scientific, French) with a 1 cm<sup>3</sup> standard quartz cell. The quantum yields of probe Rh-QL and Rh-QL with NAD(P)H at a PBS buffer solution (PH 7.4) were tested on a NanoLog infrared fluorescence spectrometer (HORIBA Scientific, USA) with an integrating sphere. Confocal imaging was conducted with a Leica TCS SP8 STED ultrahigh resolution confocal microscope (Leica, Germany). *In vivo* fluorescence imaging was obtained on the IVIS SpectrumCT *In Vivo* Imaging System (PerkinElmer, USA). Photoacoustic spectrum was collected by a Focused Half-Ring-array Photoacoustic Tomography Imaging System by 128 detectors with 2.5 MHz center frequency. The photoacoustic imaging of mice was recorded on a Focused Ring-Array Photoacoustic Tomography Imaging System.

### Synthesis of DD-QL

3-quinolinecarboxaldehyde (2.0 g, 12.7 mmol) and (1,3-Dioxolan-2-ylmethyl)triphenylphosphonium bromide(8.6 g, 20.0 mmol) were mixed with

2-(2-Methoxyethoxy)-N,N-bis[2-(2-methoxyethoxy)ethyl]ethanamine (4.2 mL, 4.3 mmol) in sat. aq.  $K_2CO_3$  (50 mL) and  $CH_2Cl_2$  (50 mL). After being heated at reflux for 6.0 h, the aqueous layer was extracted with  $CH_2Cl_2$  twice to combine organic layers, which were washed with brine, dried with  $MgSO_4$ , and concentrated. Dissolved the crude product in THF (60 mL) and stirred with 10% HCl (60 mL) for 1.0 h. After removing most of the THF in vacuo and cooled the mixture to  $0^\circ C$ , 10% NaOH was added to basify (pH > 10). Then the combined organic layers were obtained by extracted with EtOAc (3 $\times$ ), and washed with  $H_2O$ , brine, dried with  $MgSO_4$ , and concentrated. The obtained solid was purified by silica gel chromatography (hexanes : EtOAc = 1:1) to get a yellow solid product (2.0 g, 84%).  $^1H$  NMR (600 MHz, Chloroform-d)  $\delta$  9.77 (d, J = 7.5 Hz, 1H), 9.09 (d, J = 2.2 Hz, 1H), 8.30 (d, J = 2.3 Hz, 1H), 8.12 (d, J = 8.4 Hz, 1H), 7.87 (dd, J = 8.4, 1.4 Hz, 1H), 7.78 (ddd, J = 8.4, 6.8, 1.4 Hz, 1H), 7.64 (s, 1H), 7.61 (d, J = 2.1 Hz, 1H), 6.92 (dd, J = 16.1, 7.5 Hz, 1H).  $^{13}C$  NMR (151 MHz, Chloroform-d)  $\delta$  193.18, 149.36, 149.09, 148.86, 136.09, 131.33, 130.00, 129.64, 128.64, 127.80, 127.61, 127.09. HR-MS: calc. DD-QLH $^+$  [ $C_{12}H_{10}NO_2$ ] $^+$ , 184.0757, found: 184.0754.

### Synthesis of Rh-DD-Q

H1 was synthesized according to the method reported before.<sup>1</sup> The compound H1 (2 mmol) and DD-QL (1.2 equivalents) were dissolved in 15.00 mL acetic anhydride, and the mixture was stirred at  $80^\circ C$  for 6.0 h in a  $N_2$  atmosphere. TLC showed the reaction was complete. The solvent acetic anhydride was removed under reduced pressure, and the obtained solid was purified by silica gel chromatography ( $CH_2Cl_2/CH_3CH_2OH$  = 20:1) to get a green solid product (0.58 g, yield: 54%).  $^1H$  NMR (600 MHz, DMSO-d $_6$ )  $\delta$  9.20 (d, J = 2.1 Hz, 1H), 8.53 (d, J = 2.1 Hz, 1H), 8.05 (d, J = 7.9 Hz, 1H), 7.96 (d, J = 8.4 Hz, 1H), 7.93 (d, J = 8.1 Hz, 1H), 7.80 (t, J = 7.6 Hz, 1H), 7.71 – 7.65 (m, 3H), 7.57 (t, J = 7.5 Hz, 1H), 7.51 (s, 1H), 7.32 (d, J = 7.6 Hz, 1H), 7.23 (d, J = 15.3 Hz, 1H), 6.83 (s, 1H), 6.66 – 6.60 (m, 1H), 3.47 (q, J = 7.2 Hz, 4H), 2.88 (dt, J = 16.7, 4.9 Hz, 1H), 2.77 – 2.69 (m, 1H), 2.08 – 1.90 (m, 2H), 1.75 – 1.60 (m, 2H), 1.14 (t, J = 7.0 Hz, 6H).  $^{13}C$  NMR (151 MHz, DMSO-D $_6$ )  $\delta$  168.30, 150.40, 147.69, 134.78, 133.63, 130.64, 130.50, 130.41, 130.34, 129.46, 129.32, 128.88, 128.70, 128.22, 127.76, 127.31, 96.59, 45.16, 25.66, 21.65, 21.58, 13.00. HR-MS: calc. Rh-DD-Q [ $C_{36}H_{33}N_2O_3$ ] $^+$ , 541.2486, found: 541.2477.

### Synthesis of Rh-DD-QL

The compound Rh-DD-Q (0.6 mmol) was dissolved in 8.0 mL anhydrous acetonitrile, followed by adding dropwise MeOTf (1.5 equivalents). The solution was stirred at  $25^\circ C$  for 4.0 h. TLC showed the reaction was complete. After the solvent was removed under reduced pressure, the crude product was washed with cyclohexane and dried to obtain a black solid (0.15 g, yield: 27%).  $^1H$  NMR (600 MHz, DMSO-d $_6$ )  $\delta$  9.94 (d, J = 1.8 Hz, 1H), 9.41 (s, 1H), 8.48

(d, J = 8.9 Hz, 1H), 8.43 – 8.39 (m, 1H), 8.26 – 8.20 (m, 2H), 8.04 (t, J = 7.6 Hz, 1H), 8.01 – 7.93 (m, 2H), 7.90 (td, J = 8.4, 7.5, 1.9 Hz, 1H), 7.79 (td, J = 7.9, 1.4 Hz, 1H), 7.47 (d, J = 14.1 Hz, 1H), 7.42 (d, J = 7.7 Hz, 1H), 7.35 (d, J = 2.3 Hz, 1H), 7.32 (dd, J = 9.6, 2.5 Hz, 1H), 6.97 (dd, J = 9.6, 1.6 Hz, 1H), 4.65 (s, 2H), 3.70 (d, J = 7.3 Hz, 4H), 2.96 (q, J = 6.9 Hz, 2H), 2.30 (dddd, J = 40.6, 16.2, 7.1, 4.8 Hz, 2H), 1.85 – 1.75 (m, 2H), 1.27 – 1.16 (m, 6H). <sup>13</sup>C NMR (151 MHz, DMSO-D6) δ 165.81, 162.13, 159.98, 158.67, 156.29, 150.11, 143.47, 137.90, 135.92, 134.65, 134.42, 134.22, 132.02, 131.39, 131.09, 131.04, 130.34, 129.80, 129.65, 128.76, 123.79, 119.85, 119.60, 118.45, 96.11, 53.22, 46.18, 26.15, 25.56, 21.11, 12.96. HR-MS: calc. Rh-DD-QL [C<sub>37</sub>H<sub>36</sub>N<sub>2</sub>O<sub>3</sub>]<sup>2+</sup>, 278.1358, found: 278.1357.

### ***In Vitro* Detection of NAD(P)H**

Rh-DD-QL stock solution (2 mM) was prepared by dissolving Rh-QL in solvent (H<sub>2</sub>O/DMSO = 8:2). For all experiments, the stock solution of Rh-DD-QL was diluted with phosphate buffer solution (PBS, 0.01 M, pH=7.4) to give a work solution of a PBS buffer (0.01 M, pH 7.4, 0.2% DMSO) containing 20 μM Rh-DD-QL. Stock solution of NAD(P)H and various interfering reagents were prepared in water and added to the solution of Rh-DD-QL (20 μM). The time-depending spectral test started immediately after adding NAD(P)H within 0-80 min. The concentration-depending spectrum was recorded after incubation of Rh-DD-QL and NAD(P)H at 37°C for 1.0 h. The UV-vis spectra were collected from 500 nm to 900 nm, and the fluorescence spectra were recorded in a range of 780-850 nm (λ<sub>ex</sub> = 760 nm), where slit widths were 10/10 nm. The photoacoustic spectra were recorded in a range of 700-900 nm, taking 0.1 M CuSO<sub>4</sub> as a standard reference solution.

### **Measurement of quantum yield**

Fluorescence quantum yield was measured by IR-783 (Φ<sub>ref</sub> = 0.11) as a fluorescence reference. The IR-783 and reaction product (Rh-DD-QLR) were dissolved in H<sub>2</sub>O to form a dilute solution and adjusted to give the same absorbance of ca. 0.09 at 760 nm. Then, the emission spectrum was recorded at the excitation of 760 nm, and the integrated areas of the spectra were calculated. The fluorescence quantum yield was given by the following equation:

$$\Phi_s = \Phi_{ref} (A_{ref}F_s/A_sF_{ref}) (n_s/n_{ref})^2$$

Where Φ is the fluorescence quantum yield, A is the absorbance at 760 nm, F is the integral area of the fluorescence spectrum, and n is the refractive index of the solvent. The subscripts *ref* and *s* represent the reference and the analyte, respectively.

## **Cell Culture and Cytotoxicity Test**

The 4T1 cells were obtained from the National Infrastructure of Cell Line Resource and cultured in DMEM medium with 10% fetal bovine serum (FBS) at 37°C and a 5% CO<sub>2</sub> atmosphere. The third to tenth generation cells after resuscitation were seeded on confocal dishes or 96 well plates and allowed to adhere for 24.0 h before being treated. For cytotoxicity assay, 4T1 cells (10<sup>6</sup> cells/well) were incubated with different concentration (0, 25, 50, 100, and 200 μM) of Rh-DD-QL for another 12.0 h. Then the culture medium was changed and 10 μL CCK-8 solution was added to each well. After 3.0 h, the optical density at 450 nm of each well was recorded on a microplate reader. The absorbance of the cells in the medium was normalized and considered 100% viability in the control group. Meanwhile, different concentrations of Rh-DD-QL were co-incubated with 4T1 cells for 12.0 h, followed by staining with Calcein AM/PI for 0.5 h.

## **Fluorescence Imaging in living cells**

For endogenous NAD(P)H imaging of 4T1 cells, the Rh-DD-QL stock solution was added to the adherent cells to achieve a concentration of 50 μM Rh-QL, and time-dependent images were acquired after incubating for different times (0, 0.5, 1.0, 2.0, and 3.0 h). To obtain exogenous NAD(P)H images of 4T1 cells, the cells were cultured in different concentrations of NAD(P)H (0, 0.25, and 1.0 mM) for 0.5 h and then stained with 50 μM Rh-DD-QL for 1.0 h. For the mitochondrial-colocalization assay, the cells were treated with 50 μM Rh-DD-QL for 0.5 h, followed by being co-stained with 50 μM Rh-DD-QL and 10 μM Mito-Tracker Green for 0.5 h. To obtain NAD(P)H images in the energy metabolism of 4T1 cells, the cells were pre-treated with 0-50 mM glucose before incubating with 50 μM Rh-DD-QL for 1.0 h. For NAD(P)H imaging in the EGCG treatment, the 4T1 cells were pre-treated with 0-100 μM EGCG for 6.0 h and then treated with 50 μM Rh-DD-QL for another 1.0 h. For Cell viability test in the EGCG treatment, the 4T1 cells were treated with 0-100 μM EGCG for 48.0 h.

All cells were washed with PBS buffer three times after being stained. Except that the mitochondrial-colocalization assay used a 63× objective lens, all images were collected on a confocal fluorescence microscope with a 20× objective lens, using 670 nm excitation, 700-800 nm emission filters in Rh-DD-QL imaging, and 488 nm excitation, 500-640 nm emission filters in Mito-Tracker Green imaging (green channel).

## **Tumor Mouse Model**

All animal experiments were carried out strictly according to the regulations issued by the laboratory animal research center of Tsinghua University (LQL23-1). Female BALB/c nude mice aged 5 weeks were randomly selected to be injected with 4T1 cells (1×10<sup>7</sup>, suspended in DMEM medium) into subcutaneous to establish a subcutaneous tumor model in their buttocks. After 7

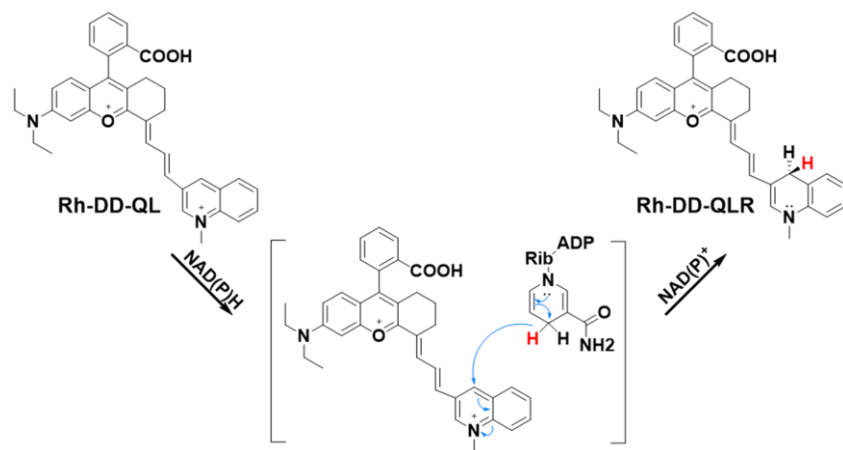
days, normal mice were divided into three groups named H<sub>1</sub>, H<sub>2</sub>, and H<sub>3</sub>. Meanwhile, tumor-bearing mice were divided into four groups named C<sub>1</sub>, C<sub>2</sub>, C<sub>3</sub>, and C<sub>4</sub> randomly and respectively.

### **Fluorescence and Photoacoustic Imaging *in vivo***

The group H<sub>1</sub>, and C<sub>1</sub> were treated with 50  $\mu$ L PBS buffer, the group H<sub>2</sub>, and C<sub>2</sub> were injected with 50  $\mu$ L PBS buffer containing 60  $\mu$ M Rh-DD-QL and the group H<sub>3</sub>, and C<sub>3</sub> were injected with 50  $\mu$ L PBS buffer containing 60  $\mu$ M Rh-DD-QL and 80  $\mu$ M NAD(P)H. In the glycolysis test, the group C<sub>4</sub> were injected with 50  $\mu$ L PBS buffer containing 60  $\mu$ M Rh-DD-QL and 40 mM D-glucose. All the above mice were injected subcutaneously and were anesthetized with isoflurane to remain anesthetized throughout the imaging process. The near-infrared fluorescence imaging of mice was performed by IVIS SpectrumCT *In Vivo* Imaging System with 780 nm excitation and 820 nm emission. Meanwhile, the photoacoustic imaging of mice was recorded on a Focused Ring-Array Photoacoustic Tomography Imaging System by 256 detectors with 5.5 MHz center frequency. The laser pulse width was 10 nanoseconds, and the imaging frequency was 10 Hz.

### **Histology analysis**

Histological analysis was performed after the above treatment. The major organs (hearts, livers, spleens, lungs, and kidneys) were immersed in 4% paraformaldehyde solution and then embedded in paraffin. These tissue sections were stained with hematoxylin and eosin (H&E) and then observed by an optical microscope.



**Scheme S1.** Proposed mechanism of probe Rh-DD-QL response to NADPH

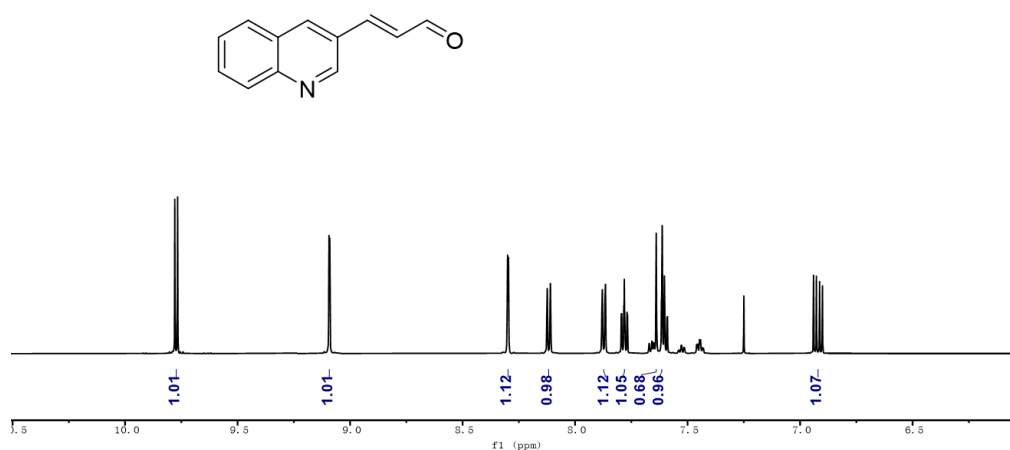


Figure S1. <sup>1</sup>H NMR spectra (600 MHz, Chloroform-d) of compound DD-QL.

yhj

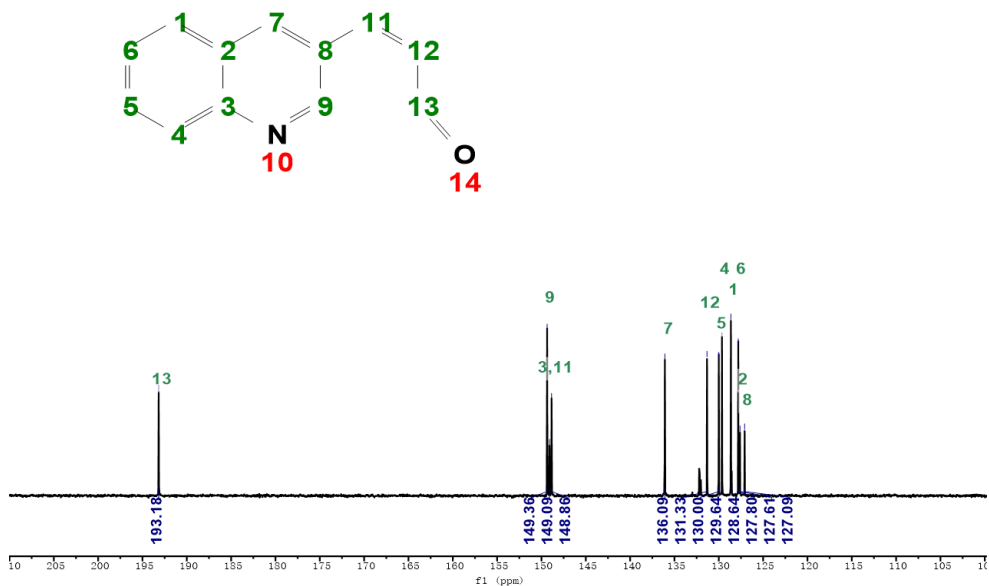


Figure S2. <sup>13</sup>C NMR spectra (151 MHz, Chloroform-d) of compound DD-QL.

3D #33-57 RT: 0.17-0.30 AV: 25 NL: 5.74E8  
T: FTMS + p ESI Full ms [100.0000-1500.0000]

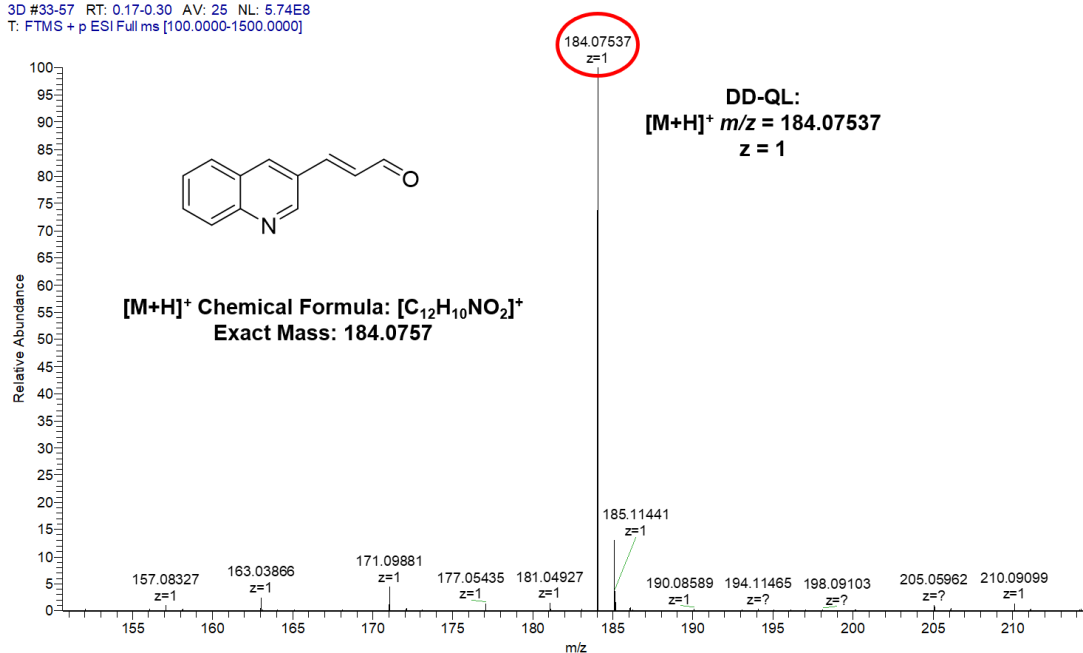


Figure S3. ESI-MS spectra of compound DD-QL. Calculated for [C<sub>12</sub>H<sub>10</sub>NO<sub>2</sub>]<sup>+</sup>: 184.0757, found: 184.0754.

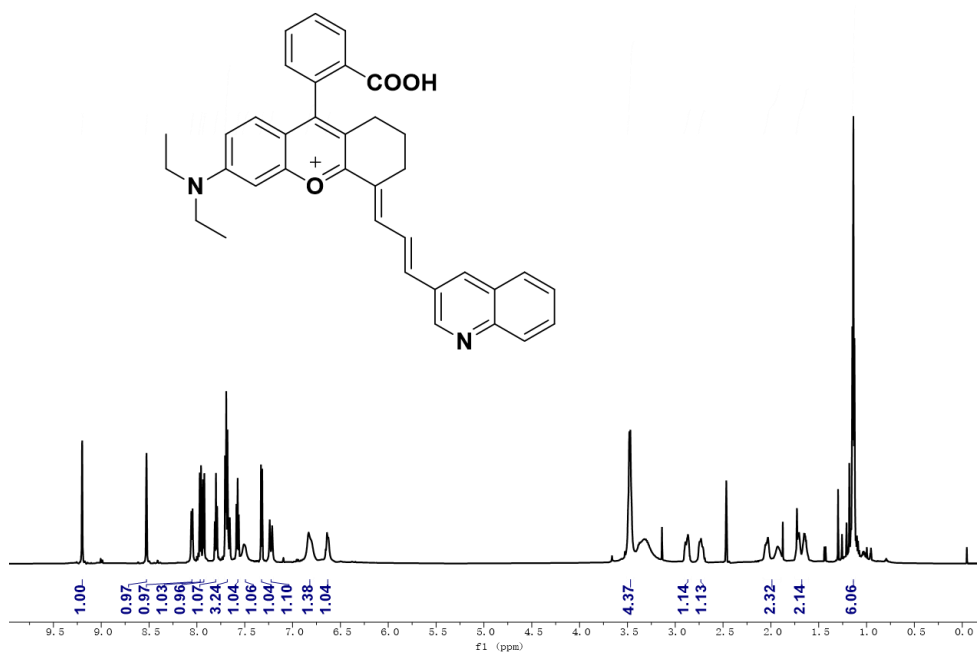
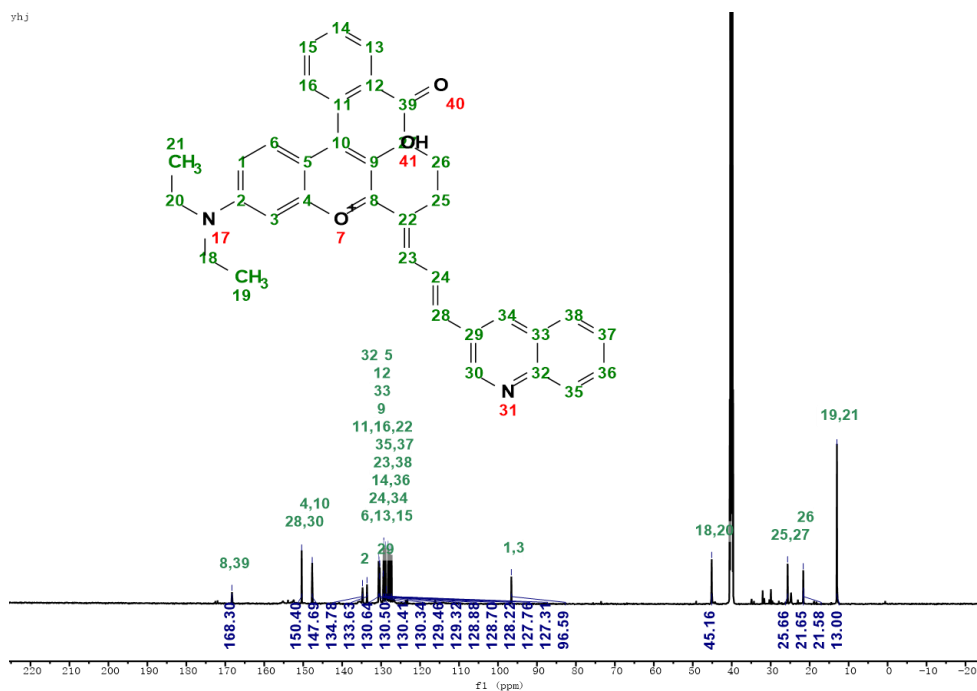
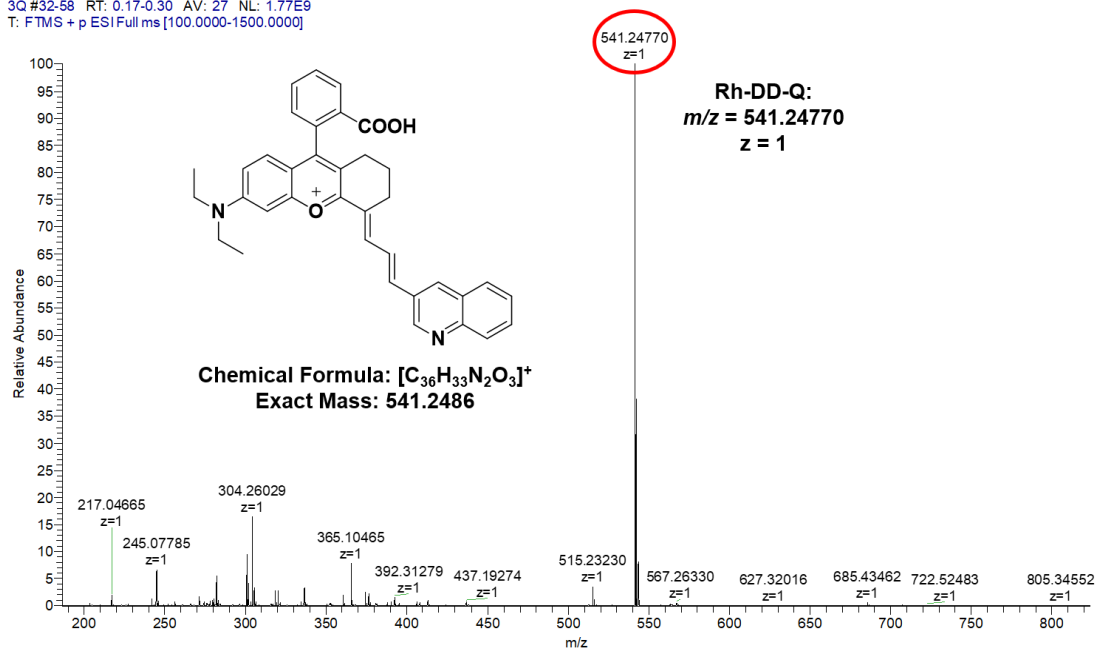


Figure S4. <sup>1</sup>H NMR spectra (600 MHz, DMSO-d<sub>6</sub>) of compound Rh-DD-Q.



**Figure S5.**  $^{13}\text{C}$  NMR spectra (151 MHz, DMSO- $\text{D}_6$ ) of compound Rh-DD-Q.

3Q #32-58 RT: 0.17-0.30 AV: 27 NL: 1.77E9  
T: FTMS + p ESI Full ms [100.0000-1500.0000]



**Figure S6.** ESI-MS spectra of compound Rh-DD-Q. Calculated for  $[\text{C}_{36}\text{H}_{33}\text{N}_2\text{O}_3]^+$ : 541.2486. Found: 541.2477.

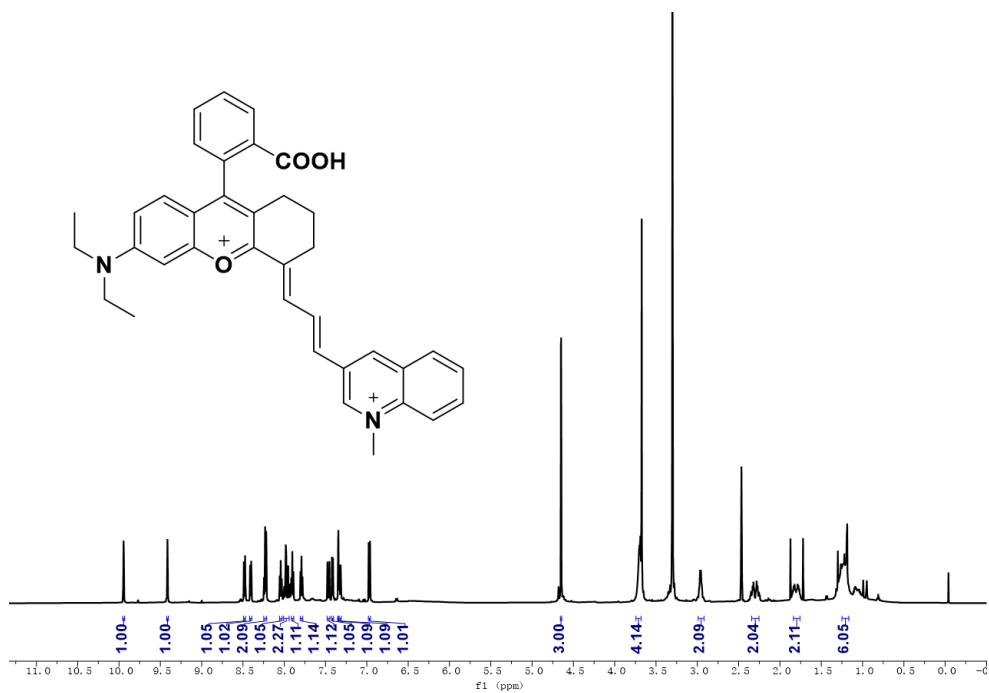


Figure S7. <sup>1</sup>H NMR spectra (600 MHz, DMSO-d<sub>6</sub>) of compound Rh-DD-QL.

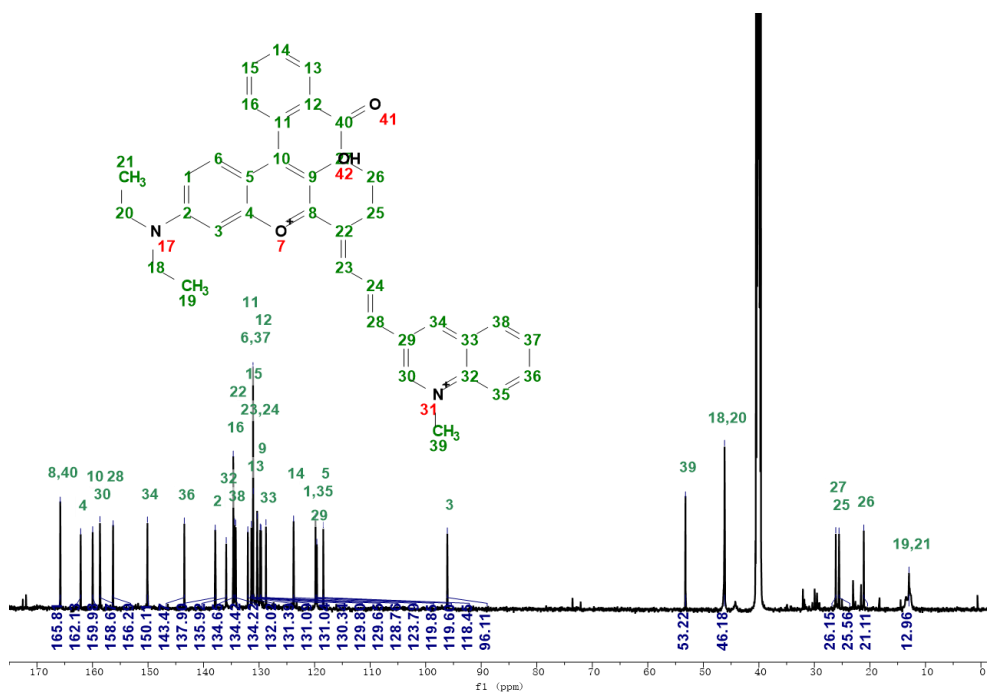
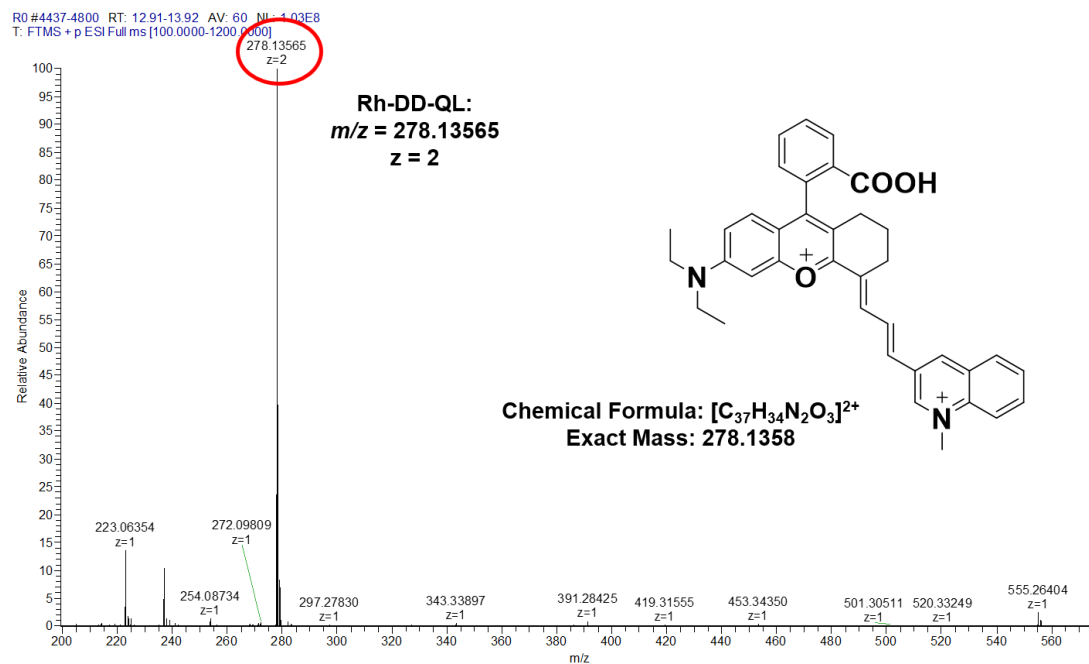
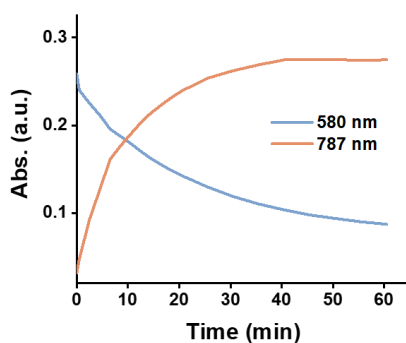


Figure S8. <sup>13</sup>C NMR spectra (151 MHz, DMSO-D<sub>6</sub>) of compound Rh-DD-QL.



**Figure S9.** ESI-MS spectra of compound Rh-DD-QL. Calculated for  $[C_{37}H_{36}N_2O_3]^{2+}$ : 278.1358. Found: 278.13565.



**Figure S10.** line profile analysis for the time-dependent UV-vis absorption intensity changes of Rh-DD-QL (20  $\mu$ M) with 200  $\mu$ M NADPH in PBS buffer (0.01 M, pH 7.4, 0.2% DMSO) from 0-1.0 h at 570 nm (blue) and 787 nm (orange).

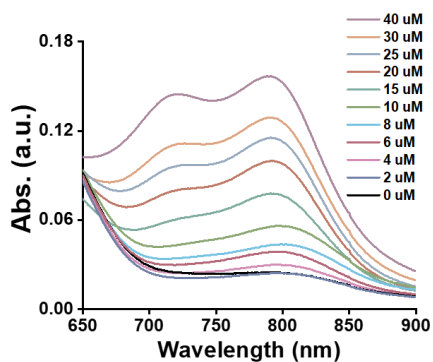


**Figure S11.** Dose-dependent UV-vis absorption spectrum changes of Rh-DD-QL (20  $\mu$ M) with increased NAD(P)H from 0 to 40  $\mu$ M in PBS buffer (0.01 M, pH 7.4, 0.2% DMSO).

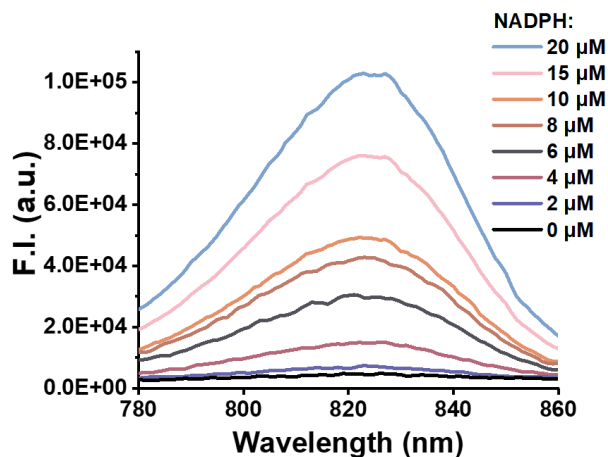


**Figure S12.** Fluorescence intensity changes of Rh-DD-QL (20  $\mu\text{M}$ ) with NAD(P)H (0-20  $\mu\text{M}$ ) in PBS buffer (0.01 M, pH 7.4, 0.2% DMSO) upon excitation at 760 nm.

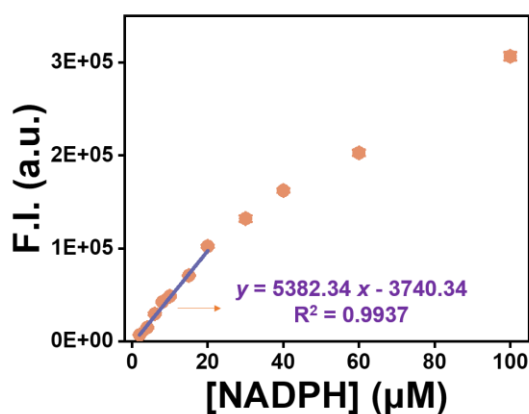


**Figure S13.** Fluorescence intensity changes of Rh-DD-QL (20  $\mu\text{M}$ ) with NAD(P)H (0-100  $\mu\text{M}$ ) in PBS buffer (0.01 M, pH 7.4, 0.2% DMSO) at 825 nm.

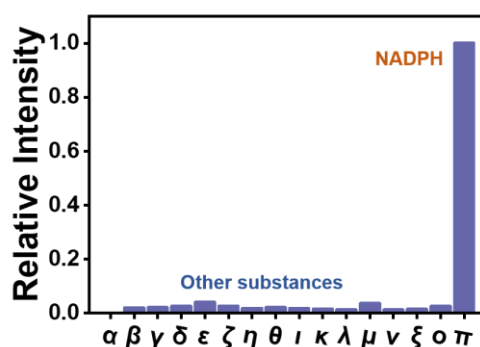


**Figure S14.** Relative absorption intensity of Rh-DD-QL at 790 nm in the presence of various analytes: 500  $\mu\text{M}$  ( $\alpha$ ) blank, ( $\beta$ ) AMP, ( $\gamma$ ) GMP, ( $\delta$ ) IMP, ( $\epsilon$ ) UDPG, ( $\zeta$ ) UTP, ( $\eta$ ) CTP, ( $\theta$ ) GDP, ( $\iota$ ) GTP, ( $\kappa$ )  $\text{Na}^+$ , ( $\lambda$ ) Lys, ( $\mu$ ) DTT, ( $\nu$ ) Gln, ( $\xi$ ) Ser, ( $\omicron$ ) Pancreatin, ( $\pi$ ) NADPH in PBS buffer (0.01 M, pH 7.4, 0.2% DMSO).

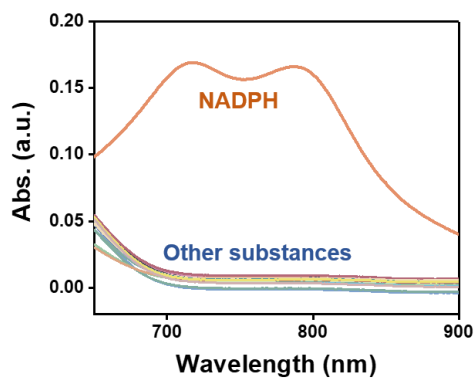


**Figure S15.** UV-vis absorption spectrum of Rh-DD-QL (20  $\mu$ M) with NADPH (orange) and other substances in PBS buffer (0.01 M, pH 7.4, 0.2% DMSO) from Figure 1F and S13.

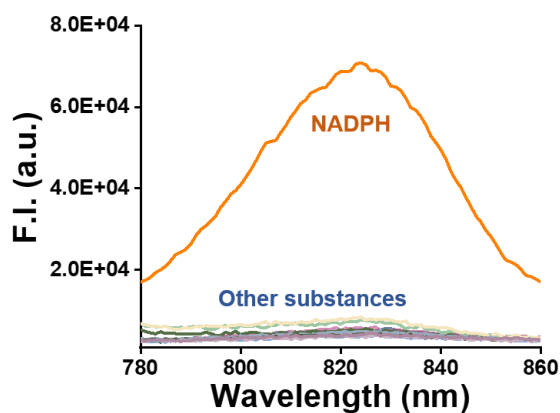


**Figure S16.** Fluorescence-emission spectra of Rh-DD-QL (20  $\mu$ M) with NADPH (orange) and other substances in PBS buffer (0.01 M, pH 7.4, 0.2% DMSO) from Figure 1F and S13.

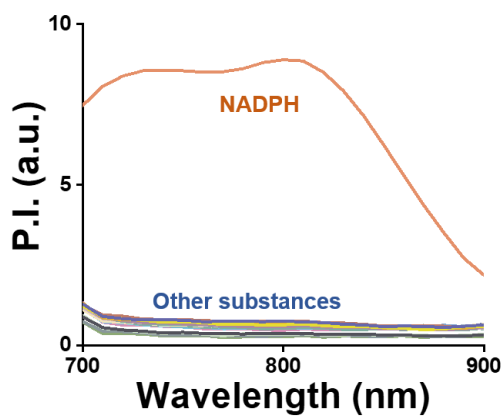


**Figure S17.** Photoacoustic spectrum of Rh-DD-QL (20  $\mu$ M) with NADPH (orange) and other substances in PBS buffer (0.01 M, pH 7.4, 0.2% DMSO) from Figure 1F and S13.

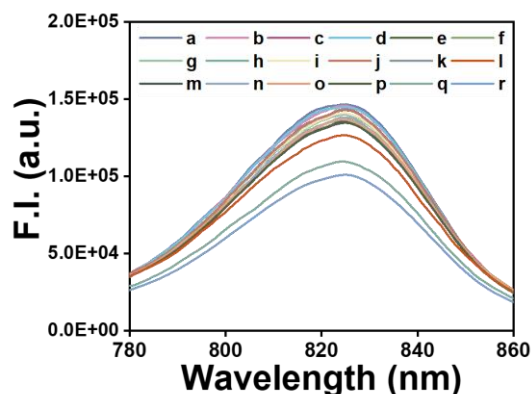


**Figure S18.** Fluorescence-emission spectra of 20  $\mu\text{M}$  Rh-DD-QL in the presence of 500  $\mu\text{M}$  various analytes ((a) Blank, (b) ATP, (c) ADP, (d)  $\text{NADP}^+$ , (e) malic acid, (f) a-ketoglutaric acid, (g) isocitrate, (h) sodium citrate, (i) Glu, (j) EGCG, (k)  $\text{NO}_2^-$ , (l) Cys, (m)  $\text{H}_2\text{O}_2$ , (n) Lys, (o) GMP, (p) GDP, (q) GSH, (r)  $\text{SO}_3^{2-}$ ) with 100  $\mu\text{M}$  NADPH in PBS buffer (0.01 M, pH 7.4, 0.2% DMSO).

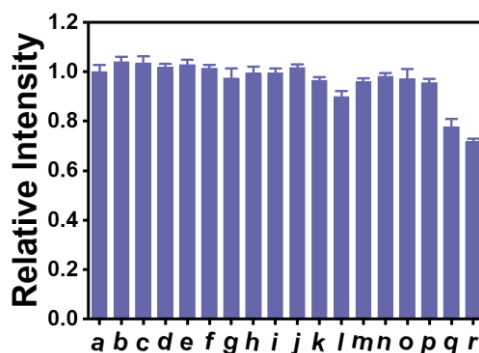


**Figure S19.** Relative fluorescence intensity of 20  $\mu\text{M}$  Rh-DD-QL in the presence of 500  $\mu\text{M}$  various analytes ((a) Blank, (b) ATP, (c) ADP, (d)  $\text{NADP}^+$ , (e) malic acid, (f) a-ketoglutaric acid, (g) isocitrate, (h) sodium citrate, (i) Glu, (j) EGCG, (k)  $\text{NO}_2^-$ , (l) Cys, (m)  $\text{H}_2\text{O}_2$ , (n) Lys, (o) GMP, (p) GDP, (q) GSH, (r)  $\text{SO}_3^{2-}$ ) with 100  $\mu\text{M}$  NADPH in PBS buffer (0.01 M, pH 7.4, 0.2% DMSO) in Figure S18. Error bars represent standard deviation ( $n = 3$ ).

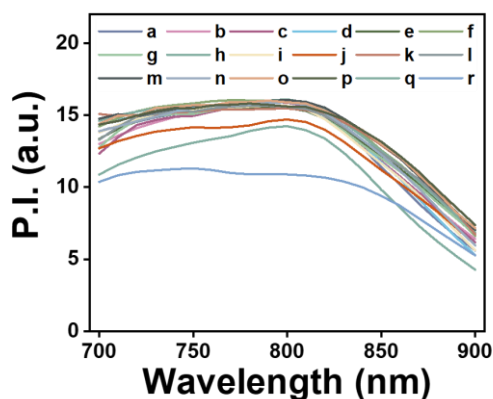


**Figure S20.** Photoacoustic spectrum of 20  $\mu\text{M}$  Rh-DD-QL in the presence of 500  $\mu\text{M}$  various analytes ((a) Blank, (b) ATP, (c) ADP, (d)  $\text{NADP}^+$ , (e) malic acid, (f) a-ketoglutaric acid, (g) isocitrate, (h) sodium citrate, (i) Glu, (j) EGCG, (k)  $\text{NO}_2^-$ , (l) Cys, (m)  $\text{H}_2\text{O}_2$ , (n) Lys, (o) GMP, (p) GDP, (q) GSH, (r)  $\text{SO}_3^{2-}$ ) with 100  $\mu\text{M}$  NADPH in PBS buffer (0.01 M, pH 7.4, 0.2% DMSO).

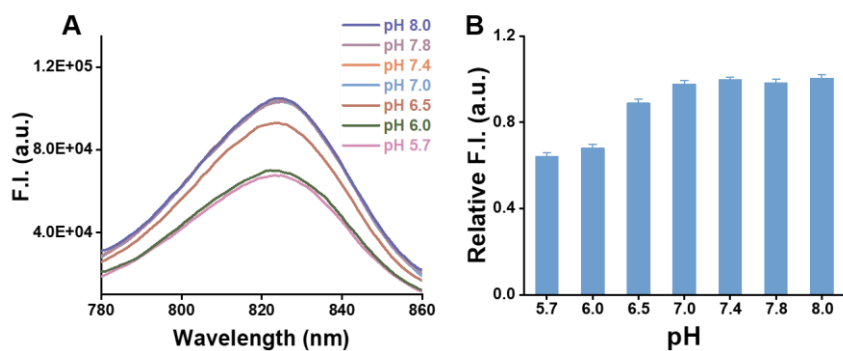


**Figure 21.** Fluorescence-emission spectra (A) and relative fluorescence intensity changes (B) of Rh-DD-QL (20  $\mu$ M) at different pH values in the presence of NADPH (100  $\mu$ M) in PBS buffer (0.01 M, pH 7.4, 0.2% DMSO) at 37°C for 1 h. Error bars represent standard deviation ( $n = 3$ ).

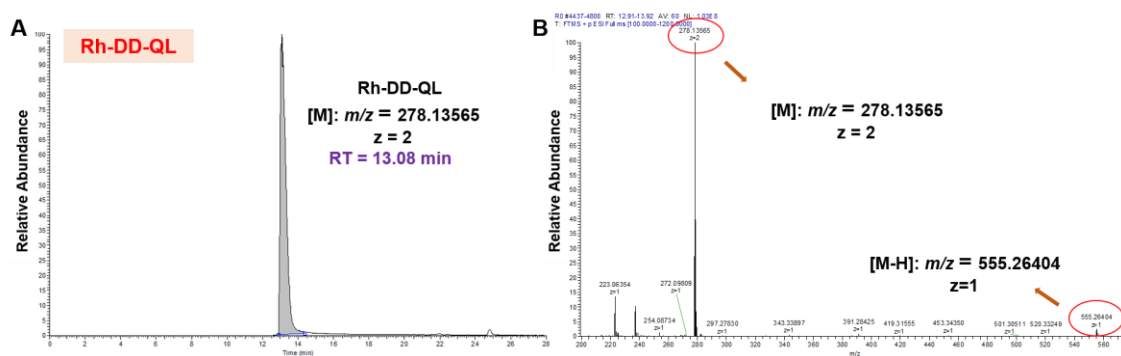


**Figure S22.** HPLC-MS spectrogram of Rh-DD-QL before addition of NADPH. Detection: UV-Vis (210, 254, 280, and 365 nm) detector. Flow rate: 0.25 mL/min. T: 30°C. Injection volume: 10  $\mu$ L. Mobile phase: 0.010-20 min: methanol-water, 5:95-100:0 (v/v); 20-28 min: 100% methanol. (B) Full scan MS spectrum for a retention time of 13.08 min in positive ion detection mode.

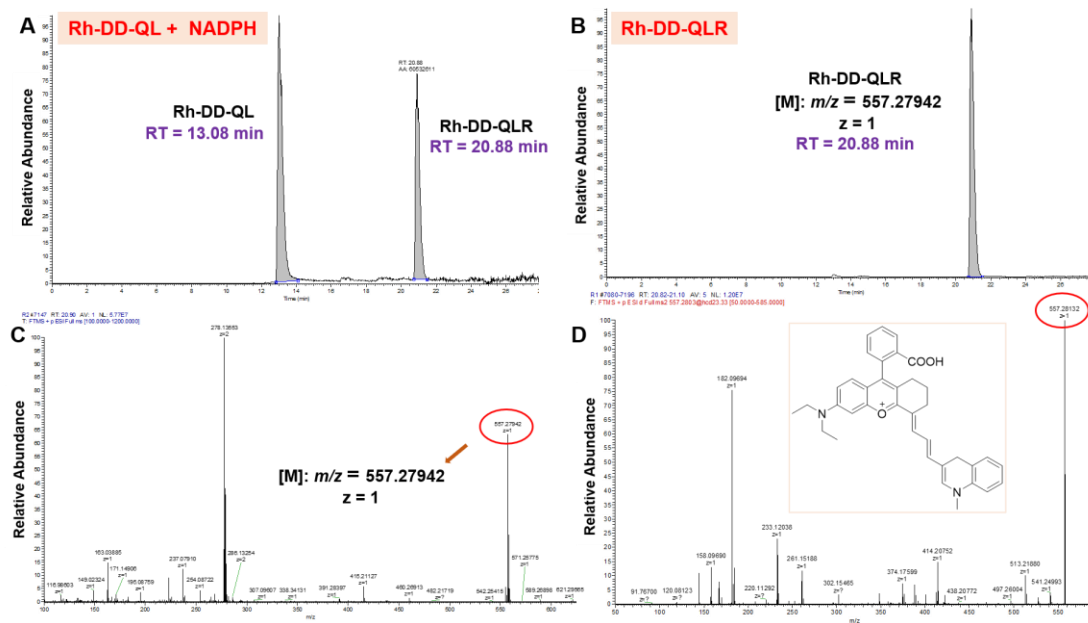


**Figure S23.** HPLC-MS spectrogram of Rh-DD-QL 1.0 h after addition of NADPH. Detection: UV-Vis (210, 254, 280, and 365 nm) detector. Flow rate: 0.25 mL/min. T: 30°C. Injection volume: 10  $\mu$ L. Mobile phase: 0.010-20 min: methanol-water, 5:95-100:0 (v/v); 20-28 min: 100% methanol. (B) HPLC-MS spectrogram of Rh-DD-QL. (C) Full scan MS spectrum for a retention time of 20.88 min in positive ion detection mode. (D) MS/MS spectrum of parent ion  $m/z = 557.279$ .

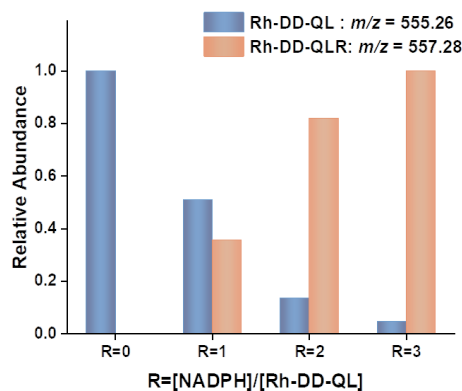


**Figure S24.** Relative abundance of Rh-DD-QL ( $m/z = 555.26$ , RT = 13.0 min) and the production of Rh-DD-QL: Rh-DD-QLR ( $m/z = 557.28$ , RT = 20.1 min) after incubation with 0, 1, 2, and 3 equivalents NADPH for 1.0 h.

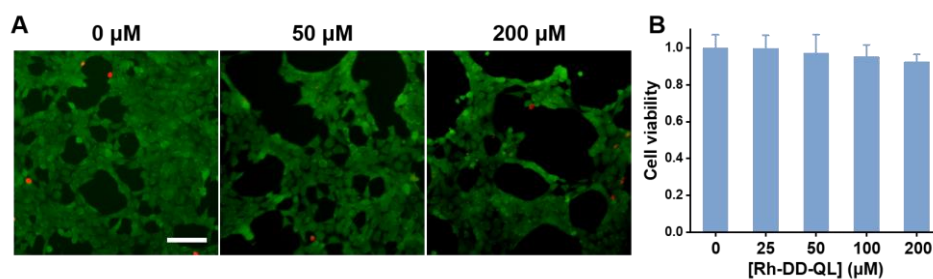


**Figure S25.** Cytotoxicity Assays of probe Rh-DD-QL. (A) Cell viability staining image of 4T1 cells incubated with 0, 50 and 100  $\mu$ M Rh-DD-QL for 12 h. (B) Relative viability of 4T1 cells incubated with various concentration of Rh-QL for 12 h. Error bars represent standard deviation ( $n = 3$ ). Scale bar: 100  $\mu$ M.

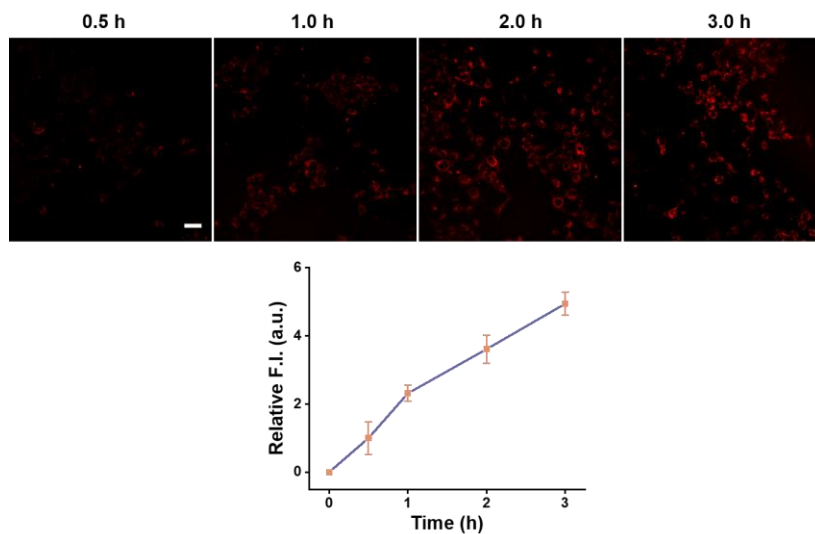


**Figure S26.** The time-dependence of cellular fluorescence images and the fluorescence intensity of 4T1 cells in the incubation of 0.5, 1.0, 2.0, and 3.0 h with 50  $\mu$ M Rh-DD-QL PBS buffer. Scale bar: 50  $\mu$ m. Error bars represent standard deviation (n = 3).

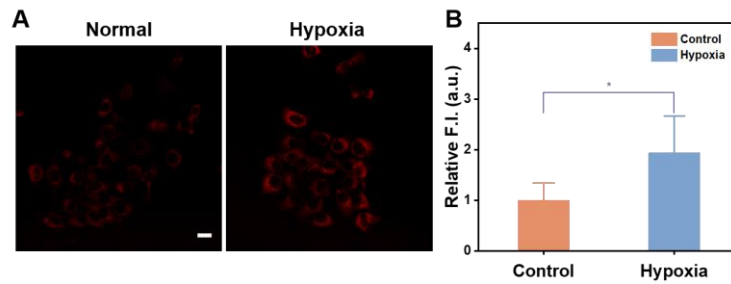


**Figure S27.** Fluorescence images and quantification of fluorescence intensities of probe (50  $\mu$ M, 1.0 h)-stained 4T1 cells cultured at normal and hypoxia atmosphere for 16.0 h. Scale bar: 20  $\mu$ m. Error bars represent standard deviation (n = 3). \*p < 0.01

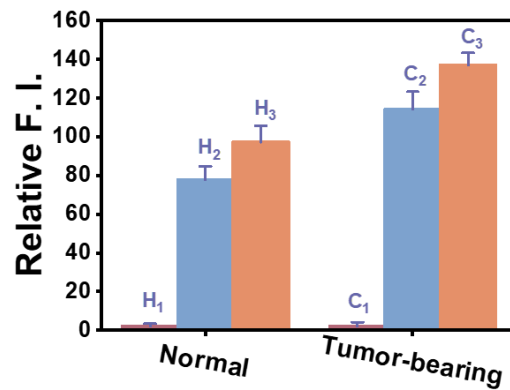


**Figure S28.** Relative fluorescence intensity of normal mice (H<sub>1</sub>, H<sub>2</sub>, H<sub>3</sub>) and tumor-bearing mice (C<sub>1</sub>, C<sub>2</sub>, C<sub>3</sub>) in Figure 4A. Error bars represent standard deviation (n = 3).

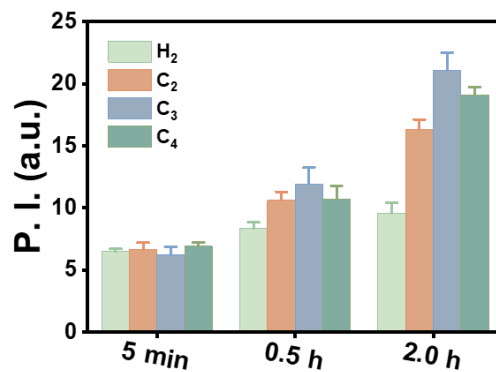


**Figure S29.** Time-dependent photoacoustic intensity variation trend of injection locations in Group H<sub>2</sub> and tumor(injection) locations in Group C<sub>2</sub>, C<sub>3</sub>, C<sub>4</sub> after orthotopic injection for 5 min-2.0 h in Figure 4C. Error bars represent standard deviation (n = 3).

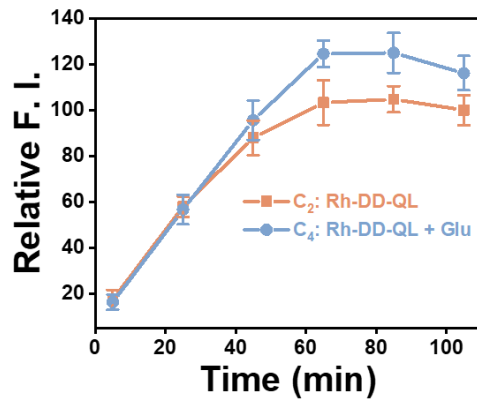


**Figure S30.** Time-dependent fluorescence intensity variation trend of tumor locations in Group C<sub>2</sub> and Group C<sub>4</sub> after orthotopic injection for 5-105 min in Figure 4B. Error bars represent standard deviation (n = 3).

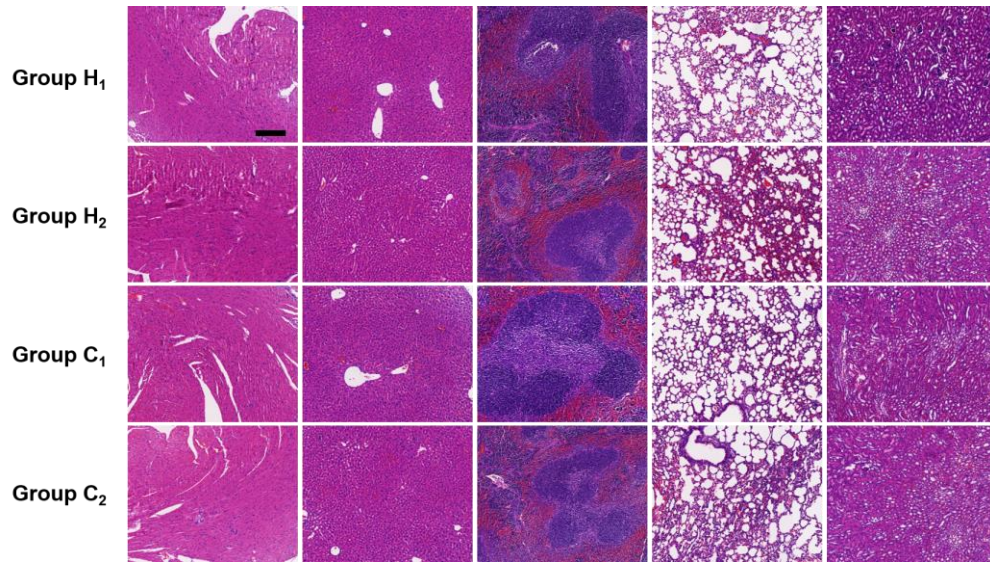


**Figure S31.** H&E-stained histological analysis of heart, liver, spleen, lung, kidney tissues obtained from the mice of the groups: H<sub>1</sub>, H<sub>2</sub> (normal mice injected with PBS buffer and Rh-DD-QL PBS buffer, respectively), C<sub>1</sub>, C<sub>2</sub> (tumor-bearing mice injected with PBS buffer and Rh-DD-QL PBS buffer, respectively). Scale bar: 200  $\mu$ m.

## Reference

L. Guan, H. Sun, J. Xiong, W. Hu, M. Ding and Q. Liang, *Sensors and Actuators B: Chemical*, 2022, **373**, 132694.